(Received 28 January 2024, Accepted 9 March 2024, Scheduled 16 March 2024)

# Multi-Band Notched Circular Polarized MIMO Antenna for Ultra-Wideband Applications

Ekta Thakur[1], Naveen Jaglan[2], Anupma Gupta[1], and Ahmed Jamal Abdullah Al-Gburi[3,*]

[1]*Department of Interdisciplinary Courses of Engineering*
*Chitkara Institute of Engineering & Technology, Chitkara University, Rajpura, Punjab, India*
[2]*Department of Electronics & Communication Engineering*
*Jaypee University of Information Technology, Waknaghat, Solan, Himachal Pradesh, India*
[3]*Center for Telecommunication Research & Innovation (CeTRI)*
*Fakulti Teknologi dan Kejuruteraan Elektronik dan Komputer (FTKEK)*
*Universiti Teknikal Malaysia Melaka (UTeM), Jalan Hang Tuah Jaya, Durian Tunggal, Melaka 76100, Malaysia*

**ABSTRACT:** This paper details the development of an innovative Ultra-Wideband (UWB) Circularly Polarized (CP) Multi-Input Multi-Output (MIMO) antenna. Drawing inspiration from an Electromagnetic Band-Gap Structure, the antenna incorporates Two Via Compact Electromagnetic Band Gap (TVCEBG) cells strategically positioned close to the feedline. The result is a sophisticated triple-band notched planar antenna configuration. To enhance its performance, a slot and a stub are strategically added to the bottom plane, effectively broadening the Axial Ratio Bandwidth (ARBW). This carefully designed setup achieves a wide ARBW while simultaneously rejecting interference at 3.5, 5.5, and 8.2 GHz. Notably, the MIMO antenna demonstrates an axial ratio spanning from 3 to 10.4 GHz, coupled with an impedance bandwidth ranging from 3.1 to 10.6 GHz. Diversity features of the proposed structure are quantified through three key parameters: ECC (Envelope Correlation Coefficient) greater than 0, TARC (Total Active Reflection Coefficient) surpassing 10, and DG (Diversity Gain) exceeding 9.7. These parameters collectively indicate robust diversity characteristics, underscoring the antenna's efficacy in challenging communication scenarios. Practical implementation involves the use of FR4 dielectric substrates, with precise measurements of $42.7 \times 55 \times 1.6\,\text{mm}^3$. This meticulous construction ensures the realization of the proposed structure's theoretical framework, highlighting the antenna's potential applicability in advanced UWB communication systems.

## 1. INTRODUCTION

High data rates are always sought by modern wireless communication systems to enhance consumer experiences. Among the benefits for data rate transfer are compact size, inclusive spectrum, and small spectral density provided by Ultra-Wideband (UWB) technology [1]. An antenna that transmits and receives polarization mismatch losses is a major challenge in such a technology. Circularly polarized (CP) antennas minimize the polarization mismatch problem by eliminating the need to align the receiving and transmitting antennas. A CP antenna can also minimize the Faraday rotation effect and multipath interference. In order to generate CP waves, two orthogonally oriented electric fields with a 90-degree phase difference can be engendered [2]. The wave can be generated by using dividers, an improved antenna structure [3], and current rotations on patch antennas. Several narrowband wireless communication systems such as WiMAX whose frequency range is between 3.3 and 3.6 GHz, WLAN whose frequency ranges from 5.1 to 6 GHz, and part of the X band whose frequency range is between 7.9 and 8.4 GHz which will cause intrusion with UWB [4]. The notch mechanism in UWB antennas is therefore essential to suppressing undesired interferences. A number of CP antennas have been discussed in the literature [5–8], but none have been designed with band-rejection capabilities. To achieve band-notch characteristics traditionally, slots are typically introduced into the antenna patch, feedline, or ground plane to disrupt and reject specific signals [9–11]. Reference [6] discusses a linearly polarized UWB antenna that employs band rejection features. UWB systems are most concerned with signal fading when operating in multipath environments. Using MIMO technology can resolve this issue by enhancing channel capacity. UWB MIMO antennas should have reduced port and field isolation. There are various types of Defected Ground Surfaces [12, 13] that can improve port isolation, including dumbbell [11, 14] and T-shaped [6] ones. It is also possible to increase mutual coupling by extending the bottom plane [15]. A dual-band notch is also proposed, with neutralization strips [15] and decoupling lines [16] for reducing isolation among the structures. To produce dual band notches, two slots are etched in the patch. There have been other approaches to achieve band-notched characteristics formed on two-dimensional resonators, such as a ring-formed resonator [10] and a wander line resonator [11]. But by removing slots from the patches, the radiation properties are further deformed. The use of Electromagnetic Band Gaps [17] (EBGs) has been proposed as a method for isolating wireless systems from unwanted interference. Wave transmission in a specific frequency range can be aided or prevented by EBG structures. In order to achieve band notch

* Corresponding author: Ahmed Jamal Abdullah Al-Gburi (ahmedjamal@ieee.org) and (ahmedjamal@utem.edu.my).

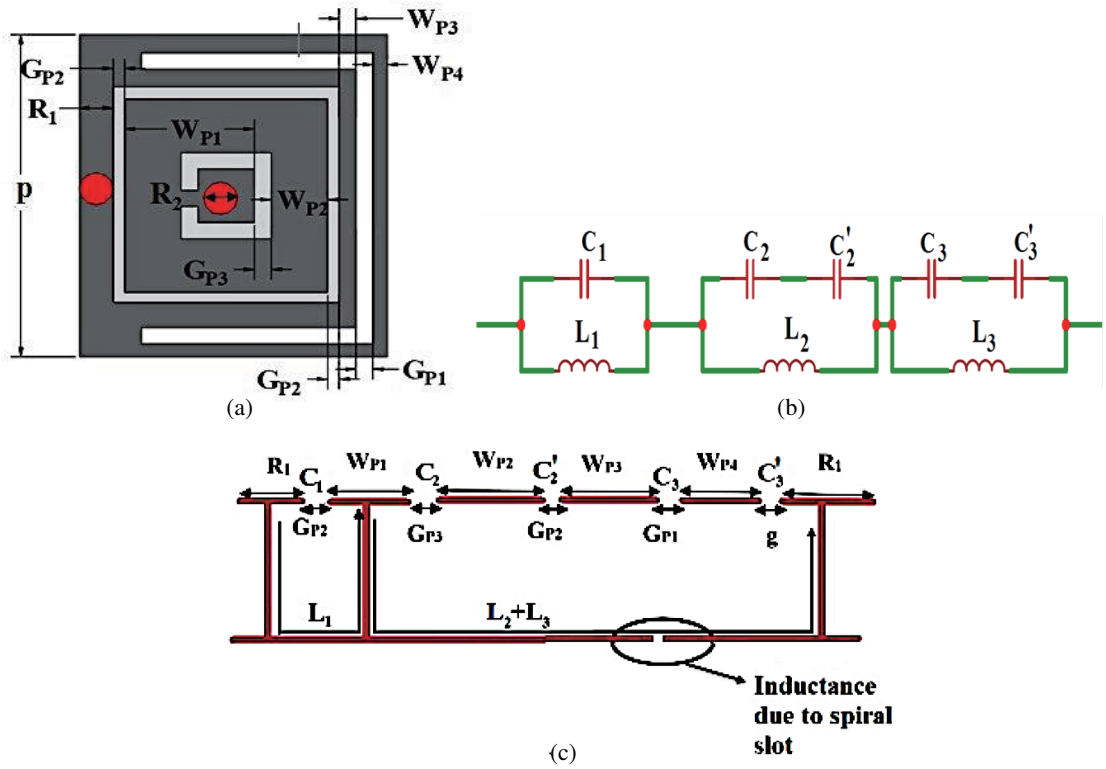


**FIGURE 1**. EBG structure. (a) TVC EBG Unit cell. (b) Equivalent circuit. (c) TVC EBG Structure aspect.

characteristics, an EBG structure with a compact footprint needs to be incorporated onto a UWB antenna. The linearly polarized UWB MIMO antenna has been designed by numerous researchers to reject dual and triple bands [11–13]. After exploring various approaches, it becomes evident that achieving a compact band-notch UWB MIMO antenna is still a challenging task.

In the suggested work, a CP MIMO antenna with triple rejected bands is presented for UWB application. The TVC-EBG structure is used next to the UWB structure's feedline to realize the three band-notches. A broad ARBW is produced by including slots beneath the feedline and extending stubs from the ground. According to the experimental results, the antenna demonstrates an impedance bandwidth that covers the range from 3 to 11 GHz, with a 3-dB extending from 3 to 10.4 GHz. The excluded frequency bands lie within the intervals of 3.3 to 3.6 GHz, 5 to 6 GHz, and 7.9 to 8.4 GHz. Meanwhile, the proposed design stands out for its compact size, straightforward design, and a more extensive ARBW than the previously discussed structures for UWB communications.

## 2. TVC-EBG STRUCTURE AND UWB ANTENNA CONFORMATION

The antenna presented in this work was constructed using a commercial FR4 substrate, characterized by a permittivity of 4.4, a height of 1.6 mm, and a loss tangent of 0.02. The modeling and simulation of the antenna were performed using HFSS (version 13).

An EBG structure functions as a filter that inhibits specific frequencies within a designated range. At the resonant frequency, EBG structures behave as surfaces with high impedance. The four structural components of the TVC-EBG are via, ground surface, dielectric, and copper patch surface. The design formulae in (1) and (2) are described in the sections underlined in [8, 17–20].

$$L = \mu_0 h \tag{1}$$

$$C = \frac{\omega\varepsilon_0\left[\varepsilon_r + 1\right]}{\pi}\text{Cos}^{-1}\left\{\frac{2w+g}{g}\right\} \tag{2}$$

$$f_c = \frac{1}{2\pi\sqrt{LC}} \tag{3}$$

where $\varepsilon_r$ = relative permittivity,
$g$ = the gap among EBG unit cell,
$w$ = patch width,
$\mu$ = relative permeability,
$\varepsilon_0$ = absolute permittivity.

To obtain a small size structure, the equivalent parameters of the inductor ($L$) and capacitor ($C$) increase in the EBG unit cell. A slot and via have been incorporated into the Electromagnetic Band Gap (EBG) unit to augment the inductance ($L$) and capacitance ($C$). In Figures 1(a)–(c), the suggested TVC EBG unit cell, equivalent circuit, and side view are depicted. Table 1 illustrates the parameter of the proposed TVC EBG structure

$$f_{c1} = \frac{1}{2\pi\sqrt{L1C1}} \tag{4}$$

**TABLE 1**. Parameter of the proposed EBG structure.

| Dimensions | $WP_4$ | $GP_1$ | $p$ | $GP_2$ | $WP_1$ | $R_1 = R_2$ |
|---|---|---|---|---|---|---|
| Units (mm) | 42.72 | 28 | 1.8 | 1.7 | 2.7 | 0.6 |
| Dimensions | $GH$ | $WP_2$ | $WP_3$ | $GP$ | $GP_3$ | $WP_4$ |
| Units (mm) | 2.29 | 1.3 | 0.3 | 0.2 | 0.3 | 0.3 |

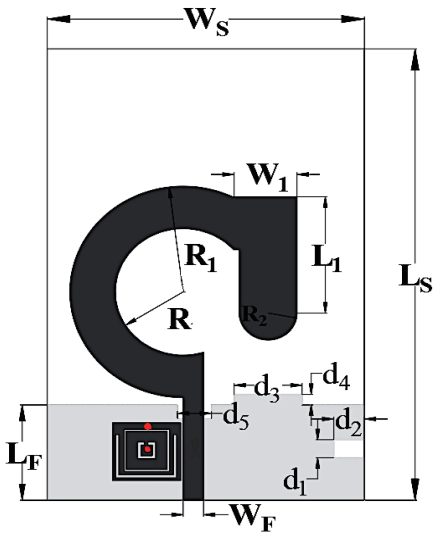


**FIGURE 2**. CP antenna's band-rejected antenna geometry.

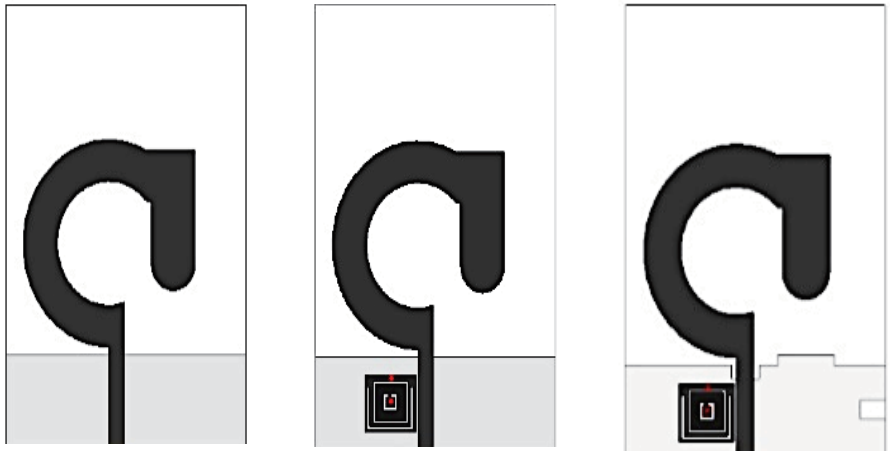

(a) Phase A (b) Phase B (c) Phase C

**FIGURE 3**. Developing steps of the proposed antenna. (a) Phase A, (b) Phase B, (c) Phase C.

**TABLE 2**. Dimensions of the proposed CP UWB structure.

| Variables | $L_s$ | $W_s$ | $W_F$ | $d_1$ | $d_2$ | $d_3$ | $d_5$ |
|---|---|---|---|---|---|---|---|
| Values (mm) | 42.72 | 28 | 1.8 | 1.7 | 2.7 | 6 | 3 |
| Variables | $W_1$ | $L_1$ | $L_f$ | $R$ | $R_1$ | $R_2$ | $d_4$ |
| Values (mm) | 5.5 | 11 | 9 | 6 | 10 | 2.5 | 1 |

$$f_{c2} = \frac{1}{2\pi\sqrt{L2C_{2eq}}} \quad (5)$$

$$f_{c3} = \frac{1}{2\pi\sqrt{L3C_{3eq}}} \quad (6)$$

### 2.1. Multi-Band Notched CP UWB Antenna

Figure 2 illustrates the prototype of the CP antenna incorporating an EBG unit cell. The CP antenna is fed by a microstrip feedline arranged in a ring shape. By strategically placing the TVC-EBG near the feedline of the UWB antenna, three rejected frequency bands can be attained. The ground plane is modified with a slot and stub to broaden the ARBW. Table 2 illustrates the dimensions of the proposed CP UWB structure. Figure 3 shows stepwise evolution of resonating antenna exhibiting triple-band rejection. Figure 3(a) illustrates an improved ring monopole with a ground surface as illustrated in Phase-A. ARBW is between 4 and 5 GHz with an axial ratio and VSWR of 3–11 GHz for Phase A. Three notch bands are achieved in Figure 3(b) by positioning the TVC-EBG near the feedline (Phase-B). ARBW can be widened by etching stubs and slots in the ground surface shown as Phase-C. Figure 4 and Figure 5 depict the VSWR and axial ratio of different phases in the formation of the present structure. In Phase-C, VSWR curve is above the threshold value 2 for the rejected bands, and axial ratio lies above 3 dB for the notched bands.

### 2.2. CP MIMO Antenna Rejecting Three Bands

In wireless communication devices and terminals, it is essential to maintain compact antenna diameters due to limited available space [21]. Designing a two-port MIMO antenna with a compact size poses challenges, primarily stemming from issues related to radiating components, port placement, and field isolation. A prototype of the structure has been made in order to validate the simulated curves. As illustrated in Figure 6, the geometry of the MIMO antenna consists of two antennas. In terms of size, the presented antenna measures $42.7 \times 55 \times 1.6$ mm$^3$. Anechoic chambers are used to measure radiation patterns, whereas Vector Network Analyser (Agilent N5230C) is used to measure curves like VSWR and mutual coupling.

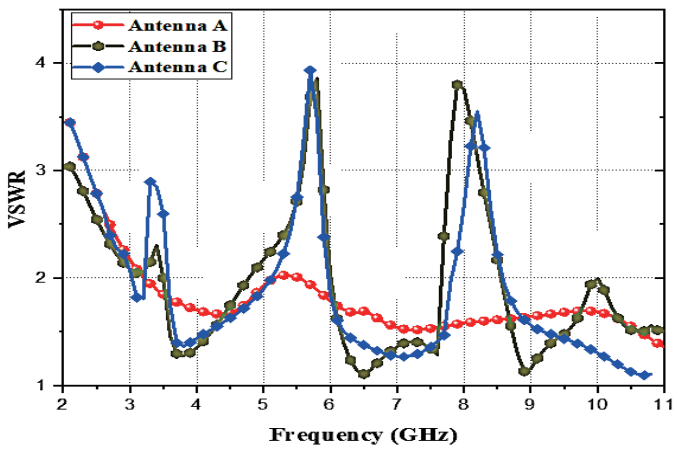


**FIGURE 4**. VSWR of different stages in the formation of the structure.

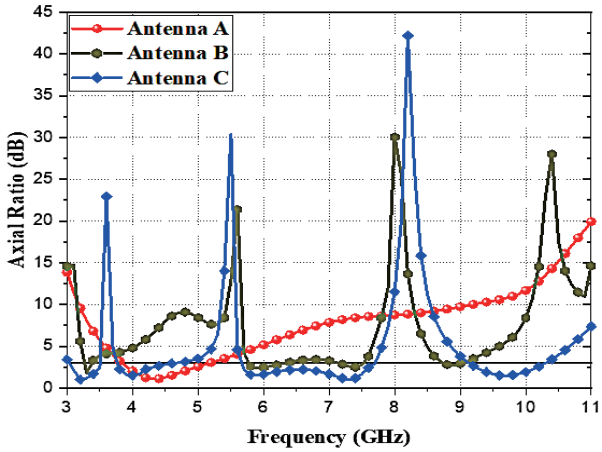


**FIGURE 5**. Axial ratio of dissimilar stages in the formation of presented structure.

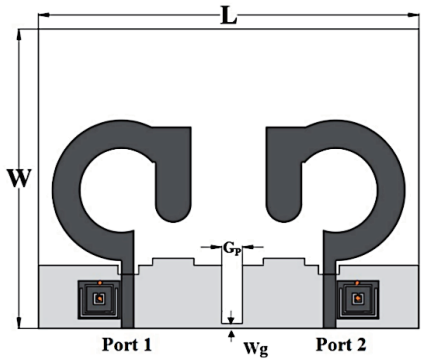


**FIGURE 6**. Antenna geometry with dimensions of 42.72 mm, 55 mm ($W \times L$).

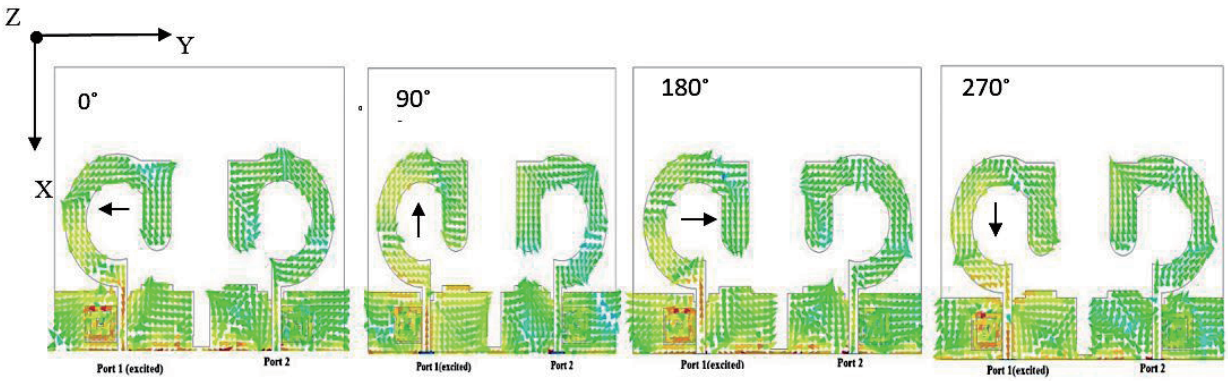


**FIGURE 7**. Port 1 Surface current is acting as circular polarized mode.

### 2.3. Circular Polarization Generation

The suggested CP MIMO Antenna works with polarization diversity. Both right hand circular polarization (RHCP) and left hand circular polarization (LHCP) modes are generated by this type of structure. It is necessary to use surface currents in order to understand the CP of the presented antennas. Figure 7 illustrates the surface current circulation at dissimilar stages 0°, 90°, 180°, and 270°. When the angle is 0°, the major vector direction is $-Y$, while when the angle is 90°, the predominant vector direction is $-X$. 180° and 270° have vector directions inversely related to 0° and 90°. Figure 7 illustrates that the surface current moves from left to right when being observed from $+Z$. RHCP is supported by the presented antenna with Port 1. CP MIMO antennas produce LHCP when Port 2 works with the phase moving from 0° to 270° as shown in Figure 8. As a result,

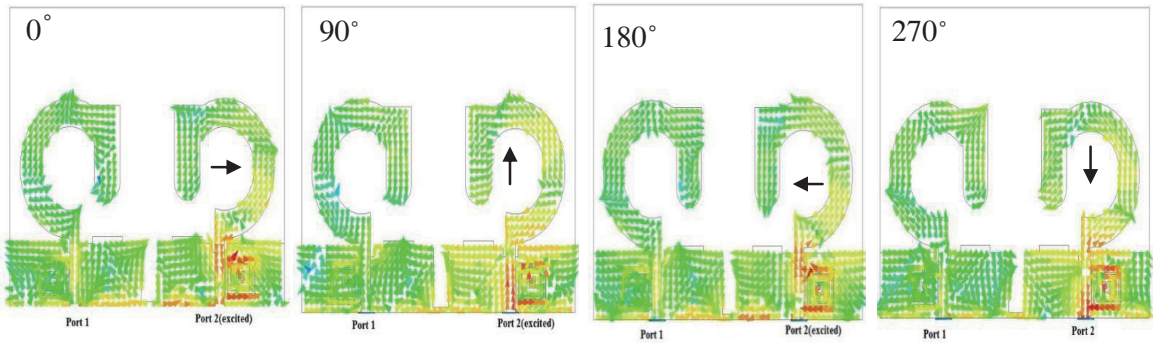


**FIGURE 8**. Port 2 Surface current is acting as circular polarized mode.

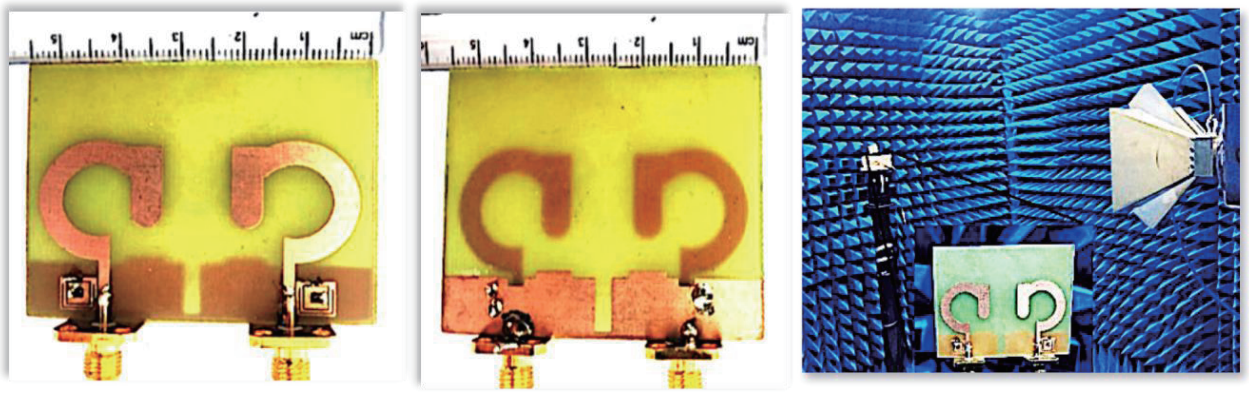

(a) (b) (c)

**FIGURE 9**. Antenna Prototype. (a) Top sight, (b) bottom sight, (c) measurement of radiation pattern in anechoic chamber.

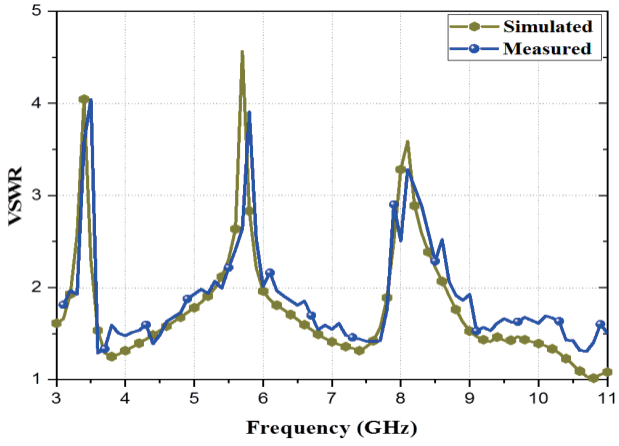


**FIGURE 10**. Tested and simulated VSWR.

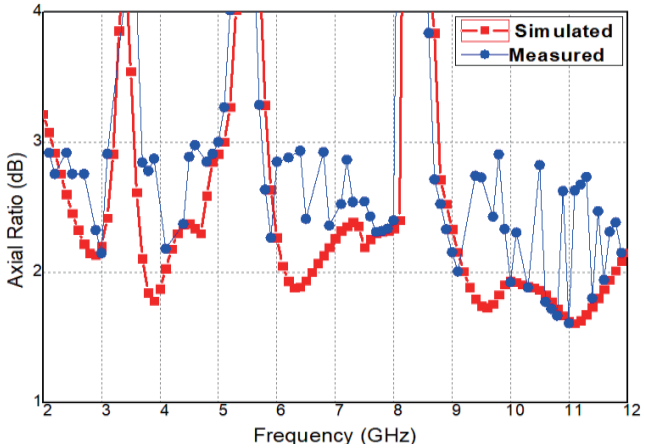


**FIGURE 11**. Tested and simulated axial ratio.

the ECC values are automatically reduced due to polarization diversity.

## 3. DISCUSSION AND RESULTS

### 3.1. Measured and Simulation Results

As depicted in Figure 9, the measurements of CP MIMO antenna prototype are made in an anechoic chamber. Figure 10 displays the simulated and measured Voltage Standing Wave Ratios (VSWRs) across the frequency range from 3.1 to 11 GHz, excluding three interfering bands. The ARBW effectively eliminates the restricted frequencies illustrated in Figure 11, covering a frequency range from 3 to 10.4 GHz. Figure 12 illustrates mutual coupling for various ground slot widths ($W_g$) ranging from 1 mm to 3 mm. Figure 13 further illustrates a corresponding increase in mutual coupling among antenna elements as $W_g$ increases. The observed trend in Figure 13 indicates that the axial ratio bandwidth decreases with an increase

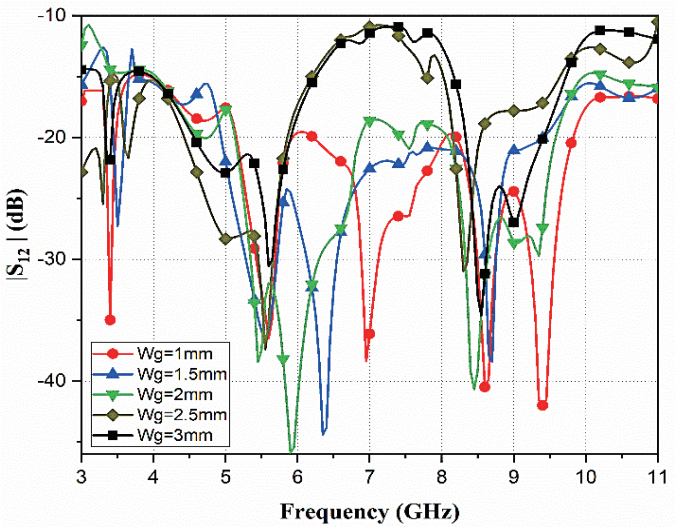


**FIGURE 12**. Deviation of isolation with dissimilar $Wg$.

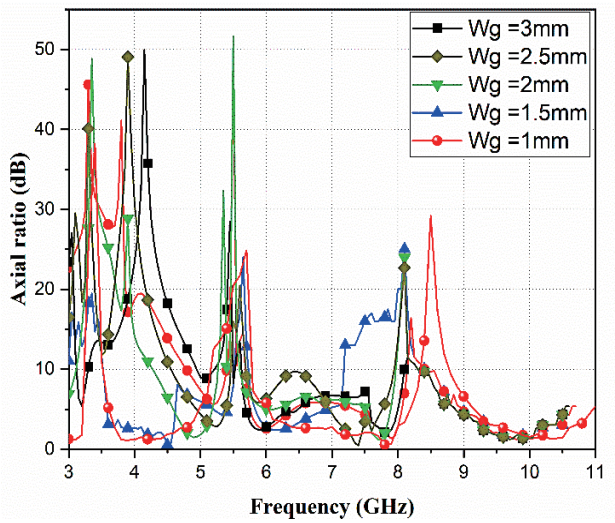


**FIGURE 13**. Deviation of axial ratio with dissimilar $Wg$.

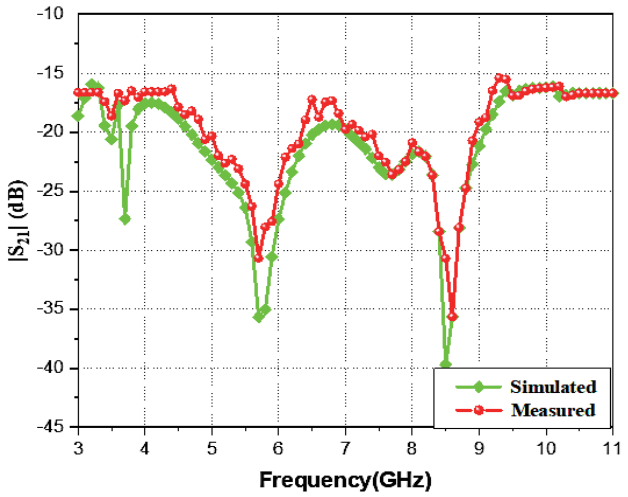


**FIGURE 14**. Deviation of the tested and simulated mutual coupling.

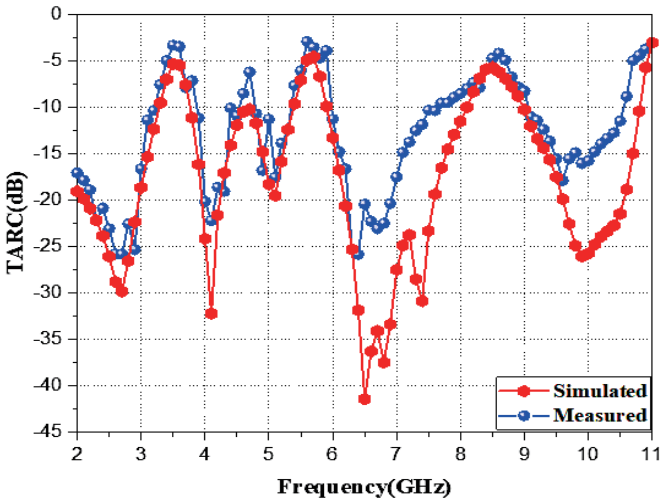


**FIGURE 15**. Deviation of the tested and simulated TARC with frequency.

in the ground slot width ($W_g$). Various losses, including conduction loss, dielectric loss, mismatch loss, and fabrication and measurement errors, contribute to discrepancies between measured and simulated parameters.

In Figure 14, the isolation between the two patches is less than 15 dB for the whole frequency range. ECC, DG, and TARC have been used to calculate MIMO performance as specified in [7, 19, 20]. Using [19], a method can be used to find ECC in an isotropic environment using scattering parameters as given below. Figure 15 illustrates the deviation of the tested and simulated TARCs with frequency. Figure 16 illustrates the results of radiation pattern measurements carried out in anechoic chambers. Only single-element antennas are considered for reflection coefficient. As specified in [22–26], TARC can be evaluated for multi-port antenna systems.

$$\text{ECC} = \frac{\left|S_{11}^{*}S_{12} + S_{21}^{*}S_{22}\right|^{2}}{\left(1-|S_{11}|-|S_{12}|\right)^{2}\left(1-|S_{21}|-|S_{22}|\right)^{2}} \quad (7)$$

$$\text{TARC} = \sqrt{\frac{\left(S_{11}+S_{12}\right)^{2}+\left(S_{21}+S_{22}\right)^{2}}{2}} \quad (8)$$

The Scattering matrix has four $S$ parameters: $S_{11}$, $S_{22}$, $S_{12}$, and $S_{21}$. Diversity gain can be assessed as recommended in [23].

$$\text{DG} = 10\sqrt{(1-|\text{ECC}|)} \quad (9)$$

Figure 17 shows DG values in the entire resonant band with very low ECC values. The correlation of the suggested antenna remains below 0.005 across the entire frequency band, except for the ranges from 3.3 to 3.6 GHz, 5 to 6 GHz, and 7.9 to 8.4 GHz, where the ECC increases to 0.03.

### 3.2. CP MIMO Antenna Comparison

Table 3 illustrates the comparability of a number of CP MIMO antennas with the presented antenna, including dimensions, the number of rejected bands, ARBW, and impedance bandwidth. From the table, it is evident that [9] is able to achieve only two

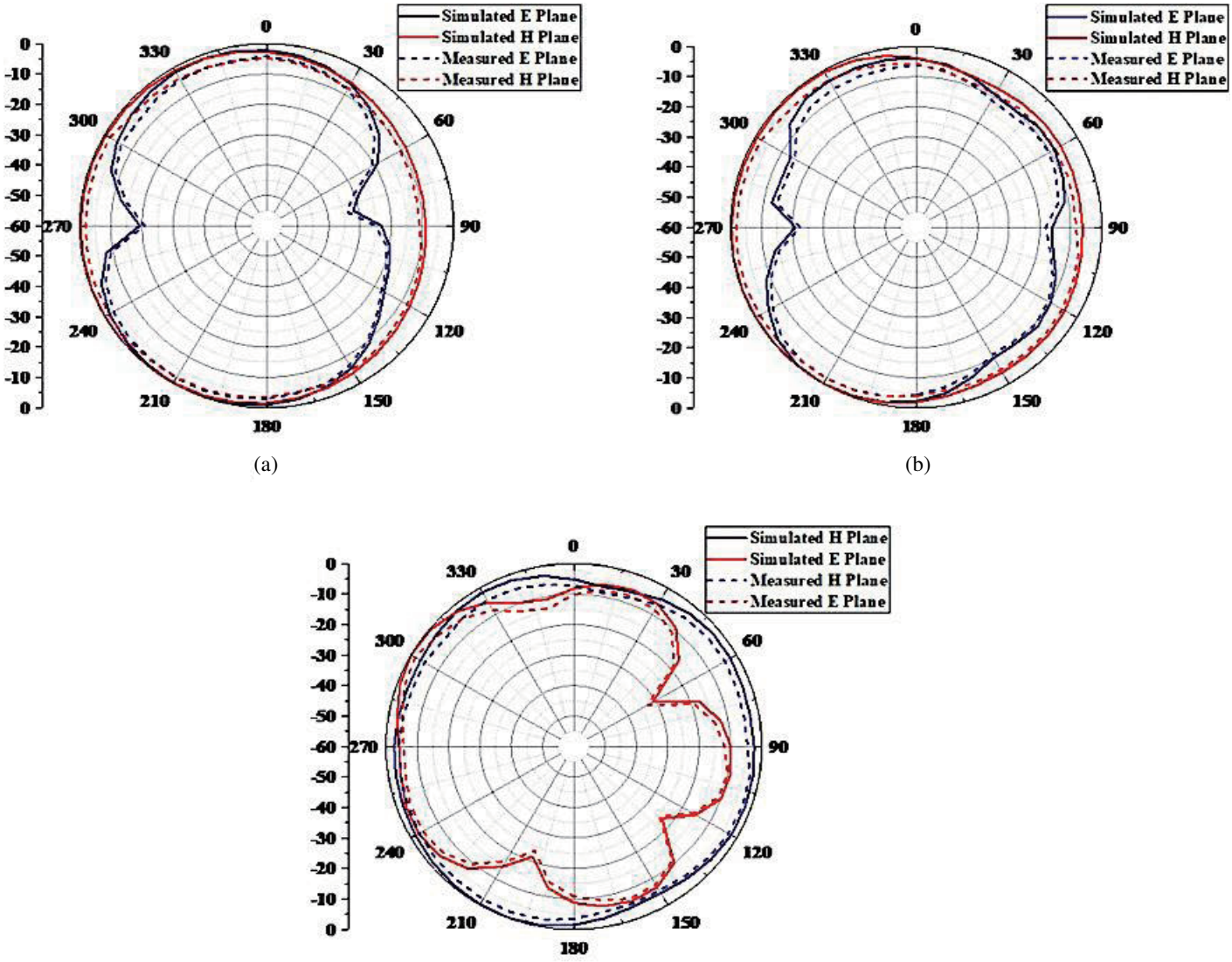


**FIGURE 16**. Standardized radiation graphs (a) at 4.0 GHz (b) 6.3 GHz (c) 7.6 GHz.

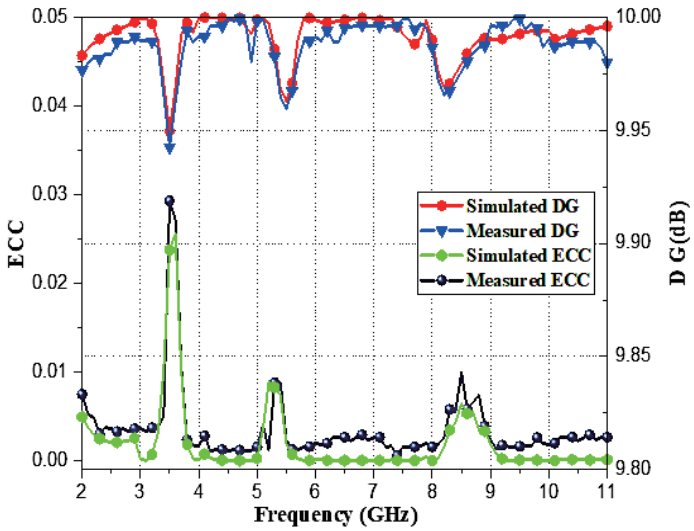


**FIGURE 17**. Measured and simulated ECC and DG of proposed system.

**TABLE 3**. Comparison of proposed structure with existing literature.

| Reference | Impedance Bandwidth (GHz) | Axial Ratio Band Width (GHz) | Number of elements | Notches (GHz) | Count of band notches | Dimensions ($mm^2$) | Mutual Coupling (dB) | Diversity Gain (DG) | Envelope Correlation Coefficient (ECC) |
|---|---|---|---|---|---|---|---|---|---|
| **Suggested Antenna** | **3–11** | **3–10.4** | **2** | **3.5, 5.5 & 8.2** | **3** | **42.72 × 55** | **-15** | **9.98 dB** | **0.005** |
| [9] | 3.2–9.6 | 3.2–8.8 | 1 | 5.2 and 5.8 | 2 | 65 × 65 | Not Available | Not Available | Not Available |
| [27] | 5.10–5.85 | 5.10–5.85 | 2 | Not Available | Not Available | 56 × 32 | −20 | 9.92 dB | **0.01** |
| [28] | 5.772–5.864 | 5.49–6.024 | 2 | Not Available | Not Available | 97 × 26.72 | −33 | Not Available | **0.01** |
| [29] | 5.8 | 5.6-6 | 2 | Not Available | Not Available | 110 × 58 | Not Available | Not Available | Not Available |
| [30] | 5.71–8.2 | 7.72–8.04 | 2 | Not Available | Not Available | 80 × 80 | −15 | 9.99 dB | **0.015** |
| [31] | 4.56–8.5 | 4.75–8.45 | 1 | Not Available | Not Available | 40 × 40 | Not Available | Not Available | Not Available |
| [32] | 5.02–10.84 | 5.07–9.22 | 1 | Not Available | Not Available | 40 × 40 | Not Available | Not Available | Not Available |
| [33] | 4.56–8.5 | 4.75–8.45 | 1 | Not Available | Not Available | 46.6 × 70 | Not Available | Not Available | Not Available |
| [34] | 1.42–2.7 | 1.42–2.7 | 1 | Not Available | Not Available | 50 × 50 | Not Available | Not Available | Not Available |

band notches, while the suggested antenna is able to achieve multiple band rejection with a simple geometry. ARBW ranges from 3 to 10.4 GHz in the suggested structure, as indicated in [9, 27–34].

## 4. CONCLUSIONS

The design and construction of a band-notched CP MIMO system for UWB and 5G applications are presented in this paper. Two of the CP antennas are placed apart from one another in order to reduce port isolation in this MIMO antenna. Additionally, TVC-EBG structures eliminate triple-narrow band frequencies and suppress three bands at center frequencies of 3.5, 5.5, and 8.2 GHz. ARWB ranges from 3 to 10.4 GHz, and impedance bandwidth ranges from 3 to 11 GHz excluding three interfering bands. With a 15 dB isolation, an ECC below 0.03, and a TARC less than 4 dB, the proposed CP MIMO structure is also capable of producing good performance when being used for MIMO scenarios. As a result, it is possible that the structure being shown can serve as the front end for the upcoming UWB-CP MIMO wireless communications devices and 5G smartphone applications.

## ACKNOWLEDGEMENT

The authors would like to express their gratitude and acknowledge the support received from Universiti Teknikal Malaysia Melaka (UTeM), the Centre for Research and Innovation Management (CRIM), and the Ministry of Higher Education of Malaysia (MOHE).

## REFERENCES

[1] Kumar, P., A. K. Singh, R. Kumar, S. K. Mahto, P. Pal, R. Sinha, A. Choubey, and A. J. A. Al-Gburi, "Design and analysis of low profile stepped feedline with dual circular patch MIMO antenna and stub loaded partial ground plane for wireless applications," *Progress In Electromagnetics Research C*, Vol. 140, 135–144, 2024.

[2] Chaudhary, P. and A. Kumar, "Compact ultra-wideband circularly polarized CPW-fed monopole antenna]," *AEU — International Journal of Electronics and Communications*, Vol. 107, 137–145, 2019.

[3] Gao, S. S., Q. Luo, and F. Zhu, *Circularly Polarized Antennas*, John Wiley & Sons, 2014.

[4] Thakur, E., N. Jaglan, S. D. Gupta, and B. Kanaujia, "A compact notched UWB MIMO antenna with enhanced performance," *Progress In Electromagnetics Research C*, Vol. 91, 39–53, 2019.

[5] Chandu, D. S. and S. S. Karthikeyan, "Broadband circularly polarized printed monopole antenna with protruded L-shaped and inverted L-shaped strips," *Microwave and Optical Technology Letters*, Vol. 60, No. 1, 242–248, 2018.

[6] Li, Y. and R. Mittra, "A three-dimensional circularly polarized antenna with a low profile and a wide 3-dB beamwidth," *Journal of Electromagnetic Waves and Applications*, Vol. 30, No. 1, 89–97, 2016.

[7] Biswal, S. P. and S. Das, "A low-profile dual port UWB-MIMO/diversity antenna with band rejection ability," *International Journal of RF and Microwave Computer-Aided Engineering*, Vol. 28, No. 1, e21159, 2018.

[8] Thakur, E., N. Jaglan, and S. D. Gupta, "Design of compact triple band-notched UWB MIMO antenna with TVC-EBG structure," *Journal of Electromagnetic Waves and Applications*, Vol. 34,

No. 11, 1601–1615, 2020.

[9] Kaur, M., H. S. Singh, and M. Agarwal, "A compact two-state pattern reconfigurable antenna for 5G Sub-6 GHz cellular applications," *AEU — International Journal of Electronics and Communications*, Vol. 162, 154577, 2023.

[10] Liu, X., J. Zhang, H. Xi, X. Yang, L. Sun, and L. Gan, "A compact four-band high-isolation quad-port MIMO antenna for 5G and WLAN applications," *AEU — International Journal of Electronics and Communications*, Vol. 153, 154294, 2022.

[11] Li, H., L. Kang, D.-W. Mi, and Y.-Z. Yin, "Simple dual band-notched UWB antenna loaded with single U-shaped resonator," *Microwave and Optical Technology Letters*, Vol. 57, No. 9, 2129–2134, 2015.

[12] Kim, J.-Y., B.-C. Oh, N. Kim, and S. Lee, "Triple band-notched UWB antenna based on complementary meander line SRR," *Electronics Letters*, Vol. 48, No. 15, 896–897, 2012.

[13] Thakur, E., N. Jaglan, and S. D. Gupta, "Ultra-wideband compact circularly polarized antenna," *Wireless Personal Communications*, Vol. 123, 407–420, 2022.

[14] Jaglan, N., S. D. Gupta, E. Thakur, D. Kumar, B. K. Kanaujia, and S. Srivastava, "Triple band notched mushroom and uniplanar EBG structures based UWB MIMO/Diversity antenna with enhanced wide band isolation," *AEU — International Journal of Electronics and Communications*, Vol. 90, 36–44, 2018.

[15] Tang, M.-C., H. Wang, T. Deng, and R. W. Ziolkowski, "Compact planar ultrawideband antennas with continuously tunable, independent band-notched filters," *IEEE Transactions on Antennas and Propagation*, Vol. 64, No. 8, 3292–3301, 2016.

[16] Zhu, J., B. Feng, B. Peng, L. Deng, and S. Li, "A dual notched band MIMO slot antenna system with Y-shaped defected ground structure for UWB applications," *Microwave and Optical Technology Letters*, Vol. 58, No. 3, 626–630, 2016.

[17] Ramachandran, A., S. V. Pushpakaran, M. Pezholil, and V. Kesavath, "A four-port MIMO antenna using concentric square-ring patches loaded with CSRR for high isolation," *IEEE Antennas and Wireless Propagation Letters*, Vol. 15, 1196–1199, 2015.

[18] Amin, F., R. Saleem, T. Shabbir, S. U. Rehman, M. Bilal, and M. F. Shafique, "A compact quad-element UWB-MIMO antenna system with parasitic decoupling mechanism," *Applied Sciences*, Vol. 9, No. 11, 2371, 2019.

[19] Nguyen Thi, T., K. C. Hwang, and H. B. Kim, "Dual-band circularly-polarised Spidron fractal microstrip patch antenna for Ku-band satellite communication applications," *Electronics Letters*, Vol. 49, No. 7, 444–445, 2013.

[20] Thakur, E., N. Jaglan, and S. D. Gupta, "Miniaturized four-port UWB MIMO antennas with triple-band rejection using single EBG structures," *International Journal of Microwave and Wireless Technologies*, Vol. 14, No. 2, 185–193, 2022.

[21] Guichi, F., M. Challal, and T. A. Denidni, "A novel dual band-notch ultra-wideband monopole antenna using parasitic stubs and slot," *Microwave and Optical Technology Letters*, Vol. 60, No. 7, 1737–1744, 2018.

[22] Yazdi, M. and N. Komjani, "Design of a band-notched UWB monopole antenna by means of an EBG structure," *IEEE Antennas and Wireless Propagation Letters*, Vol. 10, 170–173, 2011.

[23] Thakur, E., N. Jaglan, S. D. Gupta, and B. Kanaujia, "A compact notched UWB MIMO antenna with enhanced performance," *Progress In Electromagnetics Research C*, Vol. 91, 39–53, 2019.

[24] Taha-Ahmed, B. and E. M. Lasa, "Polarization diversity UWB antennas with and without notched bands," *Progress In Electromagnetics Research M*, Vol. 76, 101–111, 2018.

[25] Khan, M. S., A. D. Capobianco, S. Asif, A. Iftikhar, B. Ijaz, and B. D. Braaten, "Compact $4 \times 4$ UWB-MIMO antenna with WLAN band rejected operation," *Electronics Letters*, Vol. 51, No. 14, 1048–1050, 2015.

[26] Amin, F., R. Saleem, T. Shabbir, S. U. Rehman, M. Bilal, and M. F. Shafique, "A compact quad-element UWB-MIMO antenna system with parasitic decoupling mechanism," *Applied Sciences*, Vol. 9, No. 11, 2371, 2019.

[27] Thakur, E., N. Jaglan, and S. D. Gupta, "Design of compact UWB MIMO antenna with enhanced bandwidth," *Progress In Electromagnetics Research C*, Vol. 97, 83–94, 2019.

[28] Panahi, A., X. L. Bao, G. Ruvio, and M. J. Ammann, "A printed triangular monopole with wideband circular polarization," *IEEE Transactions on Antennas and Propagation*, Vol. 63, No. 1, 415–418, 2015.

[29] Han, R.-C. and S.-S. Zhong, "Broadband circularly-polarised chifre-shaped monopole antenna with asymmetric feed," *Electronics Letters*, Vol. 52, No. 4, 256–258, 2016.

[30] Martin, F., F. Falcone, J. Bonache, R. Marques, and M. Sorolla, "Miniaturized coplanar waveguide stop band filters based on multiple tuned split ring resonators," *IEEE Microwave and Wireless Components Letters*, Vol. 13, No. 12, 511–513, 2003.

[31] Zhang, H., Y.-C. Jiao, L. Lu, and C. Zhang, "Broadband circularly polarized square-ring-loaded slot antenna with flat gains," *IEEE Antennas and Wireless Propagation Letters*, Vol. 16, 29–32, 2016.

[32] Hu, B., Nasimuddin, and Z. Shen, "Broadband circularly polarized moon-shaped monopole antenna," *Microwave and Optical Technology Letters*, Vol. 57, No. 5, 1135–1139, 2015.

[33] Zhang, H., Y.-C. Jiao, L. Lu, and C. Zhang, "Broadband circularly polarized square-ring-loaded slot antenna with flat gains," *IEEE Antennas and Wireless Propagation Letters*, Vol. 16, 29–32, 2016.

[34] Panahi, A., X. L. Bao, G. Ruvio, and M. J. Ammann, "A printed triangular monopole with wideband circular polarization," *IEEE Transactions on Antennas and Propagation*, Vol. 63, No. 1, 415–418, 2015.